PERGAMON

International Journal of Solids and Structures 37 (2000) 2859–2882

INTERNATIONAL JOURNAL OF SOLIDS and STRUCTURES

www.elsevier.com/locate/ijsolstr

Time resolved friction during dry sliding of metal on metal

Mohammad A. Irfan, Vikas Prakash*

Department of Mechanical and Aerospace Engineering, Case Western Reserve University, Cleveland, OH 44106-7222, USA

Received 2 September 1998; received in revised form 5 April 1999

Abstract

In the present study, plate impact pressure–shear friction experiments are conducted to provide insight into time-resolved dry sliding characteristics of metal on metal at normal pressures of approximately 1.5 GPa, slip speeds up to 60 m/s and interfacial temperatures as high as 800°C. The plate impact friction experiments represent a significant improvement over conventional dynamic friction experiments by allowing control of interfacial tractions with the use of combined pressure–shear loading waves instead of manipulating actuator motion. Also, by measuring the combined normal and transverse motion of the rear surface of the target plate, critical frictional parameters such as the applied normal pressure, the interfacial slip resistance, and the interfacial slip speeds can be interpreted by using the framework of one-dimensional plane wave analysis.

The experiments are conducted on a Carpentor Hampden tool-steel (D3)/Ti–6Al–4V tribo-pair. The frictional state at the tribo-pair interface is varied by varying the impact velocity and/or the surface roughness of the impacting surfaces. Moreover, by appropriate selection of flyer and target plate thickness the tribo-pair interface is subjected to step changes in normal pressure and step changes in applied shear stress. The results of these experiments provide new insights into the evolution of interfacial sliding resistance with accumulated interfacial slip, and its dependence on surface roughness, slip velocity, normal pressure and interfacial temperature.

Keywords: Time resolved; Dynamic friction; High pressures; Elevated temperatures; Step decrements in pressure; High speed machining; Ti–6Al–4V

1. Introduction

The nature of dynamic friction forces between two bodies in contact is a complex process and is affected by a long list of factors. Most experimental apparatus employed to investigate dynamic friction lack the reproducibility of friction data. This results in multi-branched friction-stress versus slip-velocity

* Corresponding author. Fax: +1-216-368-6445.
E-mail address: vxp18@po.cwru.edu (V. Prakash).

0020-7683/00/$ - see front matter
PII: S0020-7683(99)00112-2

curves, which even for the same material and the same experimental apparatus depend not only on the properties of the frictional interface but also on the dynamic parameters of the apparatus such as mass, stiffness, and damping (Bell and Burdekin, 1969; Antoniou et al., 1976; Martins et al., 1990; Armstrong-Helouvry et al., 1994).

In the past, dynamic friction characteristics at high slip speeds and/or high normal pressures have been investigated by Ogawa (1997), Tanimura et al. (1989), Rajagopalan (1999), Rajagopalan et al. (1999), Bowden and Freitag (1958), Bowden and Persson (1960), Prakash and Clifton (1993), Prakash (1995, 1998a), to name but a few. Ogawa (1997) in his experiments modified a split Hopkinson pressure bar to study impact friction by axially impinging the input tube on a rotating output tube. Using this experimental configuration, friction experiments were conducted on a brass/brass tribo pair. The normal pressure was varied from 50 to 100 MPa and slip velocities of upto 5 m/s were obtained. But due to the relatively small time window (approximately 200 μs) slip distances were restricted to approximately 1mm. The results of these experiments indicate that when the test surfaces come in contact, the friction stress jumps to a steady state within a relatively short time of 10 to 20 μs. Moreover, the coefficient of kinetic friction is nearly independent of the normal stress for sliding speeds of up to 5 m/s. In the study by Rajagopalan et al. (1999), the conventional torsional Kolsky bar was modified to investigate dynamic friction. Using this experimental configuration, friction experiments were conducted on 6061–Al(T6)/1018 steel and 7075–Al(T6)/CH-tool-steel (D3) tribo-pairs. In these experiments the normal pressure was varied from 50 to 100 MPa. Slip velocities of up to 10 m/s were obtained and the accumulated slip distance was approximately 10 mm. The results of experiments on 6061–Al(T6)/1018 steel indicate that steady state kinetic friction is obtained within the rise time of the torsional loading pulse. The measured coefficient of kinetic friction is observed to increase with the roughness of the tribo-pair surfaces. In particular, for a soft/hard tribo-pair (7075–Al/CH-tool-steel), the surface roughness of the harder material (CH-tool-steel) is observed to control the friction force. Also, it is observed that the coefficient of kinetic friction is approximately independent of the interfacial slip velocity for sliding velocities in the range of 2 to 10 m/s and normal pressures upto 100 MPa. The experiments reported in Rajagopalan (1999) were designed to study dynamic frictional resistance of sliding interfaces in situations which involve reverse dynamic slip on a region on which slip has occurred earlier. From the results of these experiments it is observed that the dynamic friction stress required to sustain reverse slip is much higher (almost twice as large) as compared to frictional stress required for dynamic slip in the forward direction. This increase in friction stress has been attributed to the anisotropy in frictional surfaces generated during forward slip and to frictional contact of fresh metallic surfaces due to the breakdown of oxide and other surface films. In their study of high speed friction, Bowden and Freitag (1958) and Bowden and Persson (1960) spun a steel ball to a very high rotational speed and then *grabbed* it with other frictional samples or dropped it on another sample to achieve very high relative velocities (up to 800 m/s) and loads less than 0.015 MPa. In these experiments, velocity weakening of the frictional force as a function of increasing relative velocities was observed. Higher normal pressures up to 3 GPa and slip speeds up to 30 m/sec have be reported in plate impact pressure–shear friction experiments conducted by Prakash and Clifton (1993) and Prakash (1995, 1998a). In these experiments, the particle velocities at the back of a target plate struck by a flyer at an oblique angle are used to infer conditions at the frictional interface.

Recently, large scale molecular dynamics simulations of unlubricated sliding of nearly flat metal (copper) interfaces (roughness on the scale of atomic roughness) have been carried out by Roder et al. (1998) and Rigney and Hammerberg (1998). In their simulations, the interaction potentials between individual atoms are taken to be density dependent many body embedded-atom-method potentials that give a good characterization of elastic and compressive properties and defect formation energies for copper. The simulations were restricted to relative slip speeds greater than $0.01C_s$, where C_s is the speed of sound in the metal under investigation. A number of interesting results

have emerged from these simulations. In the high velocity regime, for slip velocities higher than $0.1C_s$, the coefficient of kinetic friction is found to decrease with increasing slip speeds. Associated with this velocity weakening is the evolution of microstructure in the vicinity of the sliding interface. This includes dislocation generation, dislocation motion both parallel and normal to the sliding interface, large plastic deformation, and nucleation and diffusive coarsening of microstructure with distance from the interface as time increases. As sliding proceeds, material is also observed to mechanically mix from the upper and lower regions and vice-versa, leading to a thin layer (approximately 30 atom width) of the fine grained nano-crystalline region. For slip speeds lower than $0.1C_s$, the tribo-pair materials are found to *cold-weld* together. However, by introducing nanometer scale asperities at the sliding interface, the system allows sliding even at slip speeds which had showed *cold welding* before.

The objective of the present study is aimed towards understanding the dynamic frictional characteristics of sliding interfaces under relatively high normal pressures (500 MPa to 1.5 GPa), high slip speeds (1 to 100 m/s) and elevated temperatures. Under these conditions, the material interface is expected to be essentially stable, and to a large extent from the global point of view, the frictional forces developed appear to depend primarily on the applied normal pressures, slipping velocity, slip distance, interfacial temperatures and surface roughness. This category of dynamic friction measurements encompass the general area of interfacial friction at the tool/die work-piece interface in several conventional and non-conventional material removal and/or material forming operations.

The plate impact pressure–shear friction experiment (Prakash and Clifton, 1993; Prakash, 1995; Prakash, 1998a) is especially well suited for the present investigation. A primary concern in the use of conventional dynamic friction configurations has been the influence of stiffness of the dynamic load train on the measured frictional characteristics. Additionally, there have been concerns regarding the ambiguity of the area of contact, and hence the distribution of the normal pressure at the tribo-pair interface. With the use of the plate impact pressure–shear friction experiments, the aforementioned problems associated with the measurement of dynamic friction are virtually eliminated. The use of planar pressure–shear waves to load the frictional interface results in an infinitely high loading stiffness, and any non-uniformity in geometry or alignment of the specimens result, in the worst case, in a slight spreading of the step-function load in time. This ensures uniform loading conditions over the entire contact area and the measurements truly reflect the local frictional conditions rather than being some kind of a weighted average of unknown distributions. Moreover, the plane wave loading results in a rapidly-attained steady state sliding condition with an effectively infinite loading stiffness. Consequently, changes in dynamic frictional resistance can be measured for arbitrary loading histories. Because the total slip distance is less than 250 μm, no significant wear particles are generated, making the experiment ideal for probing intrinsic dynamic slip resistance. Moreover, the principal advantage of this experimental configuration is that it allows critical frictional parameters such as the applied normal pressure, the transmitted shear stress and the interfacial slip velocity to be interpreted by using the framework of one-dimensional plane wave analysis.

The tribo-pair employed in the present investigation is CH-tool-steel/Ti–6Al–4V. The choice of the tribo-pair is dictated by its technological importance and also because of the relative high melting points of the alloys precludes at and near surface melting during the sliding process. In order to investigate the dependence of the friction stress on normal pressure and slip speed, the experiment is designed to subject the frictional interface to three well defined states: the *first state* allows investigation of dynamic sliding characteristics of the frictional interface under constant normal pressure. The *second state* allows the investigation of the sliding characteristics of frictional interfaces subjected to step changes in normal pressure. The *third state* allows the investigation of friction-stress versus slip-velocity relationship at constant normal pressures. Besides providing a fundamental insight into the evolution of interfacial sliding resistance with accumulated interfacial slip, slip velocity and normal pressure, the experimental

results provide insights for determining the structure of the rate and state-dependent dynamic friction laws.

The organization of the paper is as follows: Section 2 describes the plate impact pressure–shear friction experimental configuration and outlines the procedure used for conducting the experiments. Section 3 provides details of wave propagation in the tribo-pair plates and discusses their design considerations. Section 4 presents the wave analysis used in the interpretation to obtain the interfacial tractions, slip speeds and accumulated slip displacement. The experimental results and discussion are presented in Section 5. A summary of the main results is provided in Section 6.

2. Plate impact pressure shear friction experiment

2.1. Experimental configuration

The schematic of the plate impact pressure–shear friction experiment is shown in Fig. 1. The experiment involves the impact of a flyer plate mounted on a projectile with a stationary target plate. Impact takes place at an angle θ relative to the direction of approach, while the impacting plates are flat and parallel. This results in pressure–shear loading at the flyer–target (tribo-pair) interface. During the experiment, the impact velocity V and the normal and transverse particle velocity history of the free surface of the target plate are measured by laser interferometry. These measurements are used to infer the normal and shear tractions, slip speed, slip distance and temperatures at the frictional interface.

In all the experiments reported in the present study, the velocity and the skew angle of the projectile are controlled such that the flyer and target plates remain elastic during impact. Also, all measurements of the normal and transverse components of particle velocity at the rear surface of the target plate are made before the arrival of the unloading waves from the lateral boundaries at the monitoring point. In view of this, and during the time interval of interest, the impacting plates can be considered to be essentially infinite in their spatial dimensions and the tribo-pair to be modeled as a semi-infinite half plane sliding on another semi-infinite half-plane. This simplification in the tribo-pair geometry allows one-dimensional elastic wave theory to be used in the interpretation of the experimental results.

An 82.5 mm bore single-stage gas gun at Case Western Reserve University was used to conduct the plate impact pressure–shear friction experiments. Using this gas gun, a fiberglass projectile carrying the flyer plate is accelerated down the gun barrel by means of compressed nitrogen gas. The rear end of the projectile holds a sealing O-ring and a plastic key which slides in the key-way in the barrel to prevent rotation of the projectile. Impact occurs in a target chamber that has been evacuated to 50 μm of Hg to reduce the air cushion between the flyer and the target. The velocity of the projectile is measured to an accuracy of 1 percent or better, by recording the times at which a series of voltage biased thin wires are

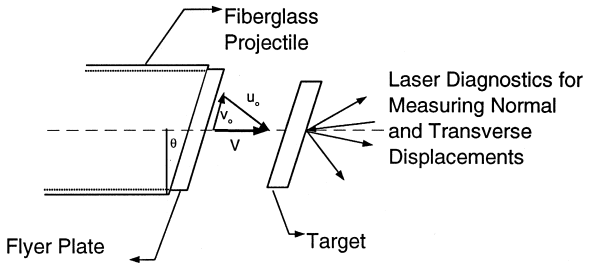

Fig. 1. Schematic of the plate impact pressure–shear friction experiment.

shorted out by contacting the flyer. To ensure generation of plane waves with wave-fronts sufficiently parallel to the impact face, the flyer and target plates are carefully aligned to be parallel to within 2×10^{-5} radians by using an optical alignment scheme developed by Kumar and Clifton (1977). The actual tilt between the two plates is measured by recording the times at which four isolated, voltage-biased pins, that are flush with the surface of the target plate, are shorted to ground. The acceptable level of tilt in the experiments is of the order of 0.5 mrads.

A laser interferometric technique is used to obtain the normal and transverse particle velocity on the rear surface of the target plate. An argon-ion laser with wavelength of 514.5 nm is used to provide a coherent monochromatic light source. Both the normal and transverse particle displacements are measured using the combined normal and transverse displacement interferometer (TDI) introduced by Kim et al. (1977). Using this interferometer, the normal displacement of the rear surface of the target plate is measured by combining a reference beam and a beam reflected from the target such that one peak to peak variation of the intensity of the light corresponds to a displacement of $\lambda/2$, where λ is the wavelength of the laser light in use. The TDI is based on the phase difference between two N^{th} order beams diffracted from a grating deposited on the rear surface of the target. The TDI sensitivity is given by $d/2n$, where d is the pitch of the diffraction grating and N is the order of diffracted beams used (in our case, $N = 1$). The interference signals are detected by photo-diodes having a rise time of less than 1 ns. The output of the photo-diodes is amplified by wide band amplifiers and then recorded on high speed digital oscilloscopes. A digital data processing program is used to process the interferometric signals and to calculate the normal and transverse particle velocities.

2.2. Tribo-pair materials and specimen preparation

The tribo-pair materials employed in the present investigation comprises a tool grade (D3) Carpenter Hampden steel and commercially available Ti–6Al–4V alloy. The Carpenter Hampden steel represents the target plate while the Ti–6Al–4V alloy represents the flyer. The physical properties of these materials are shown in Table 1. The Carpenter Hampden plates are 71 mm in diameter and approximately 6 mm in thickness while the Ti–6Al–4V plates are 76 mm in diameter and approximately 13 mm in thickness. Four copper pins, isolated electrically from the target, are placed in slots near the periphery of the impact face. The first contact of any one of these pins with the flyer provides the triggering signal for

Table 1
Physical properties of Ti6Al4V and CH tool-steel (D3)

Physical properties	Ti6Al4V	C.H. steel
Young's modulus (GPa)	110	207
Poisson's ratio	0.33	0.3
Longitudinal wave speed (mm/μs)	6.255	5.98
Shear wave speed (mm/μs)	3.151	3.264
Mass density (Kg/m^3)	4400	7860
Longitudinal impedance (GPa/mm/μs)	27.58	45.50
Shear impedance (GPa/mm/μs)	13.96	24.90
Proportional limit (MPa)	550	1600
Material hardness (HRC)	30	62
Thermal conductivity, k (W/m °K)	6	42.3
Thermal diffusivity, α (m^2/s)	2.6×10^{-6}	12.2×10^{-6}
Specific heat, C_p (J/Kg °K)	522	422

the recording system. Moreover, as mentioned earlier, these pins are used to determine the tilt between the target and flyer faces at impact.

The specimen and the flyer are lapped flat on both sides to within 2–3 Newton's rings over the diameter. Lapping is performed on a Lapmaster machine using 14.5 μm aluminum oxide powder in mineral oil. A Hommel® T500 diamond stylus surface profile measurement device is used to determine the surface roughness profiles of the lapped target and the flyer plates. To vary the surface roughness of the tribo-pair, the flyer and the target surfaces are polished on Texmeth cloth using 3 μm diamond paste. This procedure allows the surface roughness of the Carpenter Hampden steel plate to be varied from 0.02 to 0.12 μm (RMS) without losing its flatness. The corresponding range for the Ti–6Al–4V flyer plates is 0.07 to 0.18 μm.

In order to measure the combined normal and transverse particle displacement at the rear surface of the target plate, a holographic diffraction grating of 600 lines/mm is used. To fabricate the grating, one side of the target plate is lapped to a flatness of 2–3 Newton's rings over the diameter and then polished to a mirror finish using 3 μm diamond paste. After being cleaned, the surface is coated with a thin layer of Shipley Microposit® Photo resist S1813. The coated plates are then exposed to blue laser light. Two laser beams are made to intersect on the surface of the target such that they generate approximately 600 lines/mm. The grating is then developed in a mixture of one part of Shipley Microposit® developer 303A and four parts of de-ionized water. The quality of the grating is checked by monitoring the diffracted beams.

3. Design of the experiment: wave propagation in the target and flyer plates

To investigate the dynamic sliding characteristics of frictional interfaces, the thickness of the flyer and target plates are designed such that the time for longitudinal wave propagation through the thickness of the flyer plate is greater than the round-trip time of the shear wave in the target plate and the unloading waves generated at the lateral boundary. Under these conditions, when the longitudinal wave reflected from the free surface of the target plate arrives at the target/flyer interface, the normal pressure at the frictional interface is changed instantaneously. Since the longitudinal impedance of the flyer plate is less than the longitudinal impedance of the target plate, it results in a step drop in the applied normal pressure. Also, when the shear wave reflected from the target free surface arrives at the frictional interface, it produces a new frictional state while maintaining the same normal pressure. Thus, *three* distinct dynamic frictional states are obtained in each experiment.

The wave propagation in the target and flyer is illustrated schematically in the time–distance diagram shown in Fig. 2. The abscissa represents the spatial position of the wave front at any particular time and the ordinate represents the temporal location of the wave front. At impact, both longitudinal and shear waves are generated in the flyer and the target plates. In Fig. 2, the longitudinal wave fronts are represented by solid lines and the shear wave fronts are represented by dashed lines. The slope of the solid line represents the inverse of the longitudinal wave speed whereas the slope of the dashed line represents the inverse of the shear wave speed in the material. In *State 1* the tribo-pair interface is under a compressive pressure σ_1 and, depending on the interfacial resistance, a shear stress τ_1 is transmitted across the interface. Thus, *State 1* allows the investigation of dynamic sliding characteristics of the frictional interface under constant normal pressure. The first arrival of the compressive wave at the rear surface of the target plate is denoted by the letter A. Upon reflection from the rear surface of the target plate, an unloading wave is generated which propagates back towards the tribo-pair interface. When this unloading wave arrives at the frictional interface, it reduces the applied normal pressure from σ_1 to σ_2. The corresponding friction stress is denoted by τ_2. The new frictional state hence produced is called *State 2* and allows investigation of the dynamic sliding characteristics of frictional interfaces subjected to

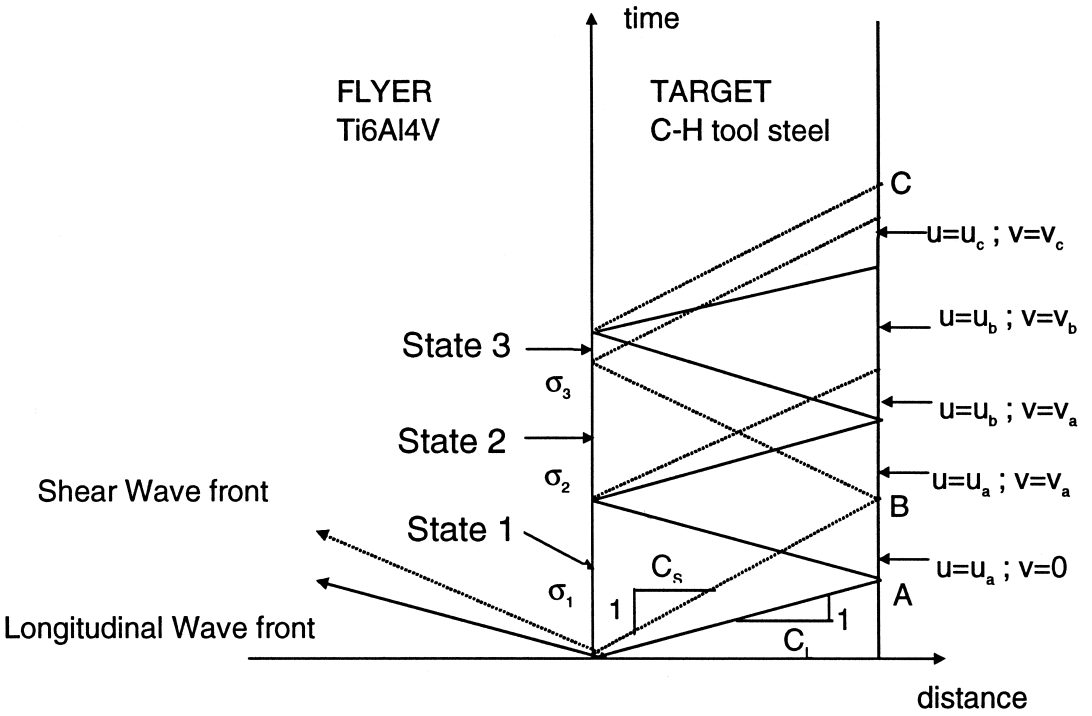

Fig. 2. Wave propagation in the flyer and target plates–time distance diagram showing the position of the stress wave fronts during the experiment.

step changes in normal pressure. The first arrival of the shear wave at the rear surface of the target plate is denoted by the letter B. The shear wave reflects from the free surface of the target plate and arrives at the frictional interface to produce a change in the applied shear stress while maintaining the same normal stress. This new friction state is denoted as *State 3*. The corresponding friction stress and slip velocity are denoted by τ_3 and V_3^{slip}, respectively. Thus, *State 3* allows investigation of the interfacial friction-stress versus slip-velocity relationship at constant normal pressure.

For the Ti–6Al–4V/CH steel tribo-pair employed in the present experiments, the duration of State 1 is approximately 1900 ns, followed by State 2 of duration 1600 ns and State 3 of duration 300 ns. During the transition from State 1 to State 2, the normal pressure, $\sigma_2 \approx 0.33\sigma_1$.

4. Wave-analysis of pressure–shear friction experiments: calculation of interfacial tractions, slip velocity and slip distance

Using the method of characteristics for 1-D hyperbolic wave equations, the components of traction at the frictional interface, the slip velocity and the accumulated slip displacement can be related to the normal and transverse components of the measured free surface particle velocity history of the target plate, $u_{\text{fs}}(t)$ and $v_{\text{fs}}(t)$, respectively, and the shear and longitudinal impedances (ρc_1) and (ρc_2), respectively.

4.1. State 1

Before impact, the flyer and the target plates are unstressed. The target is held stationary while the flyer is accelerated and impacts the target at a measured velocity V. From the knowledge of the angle of inclination θ of the projectile, the initial normal and transverse particle velocities u_0 and v_0, respectively, of the flyer plate are given by

$$u_0 = V\cos\theta \text{ and } v_0 = V\sin\theta. \tag{1}$$

When the flyer impacts the target, both normal and transverse components of velocity are imposed on the impact face. A longitudinal compression stress wave with wave speed c_1 and a shear (transverse) stress wave with a wave speed c_2 propagates into the flyer and the target plates. From one dimensional analysis of the governing hyperbolic partial differential equations, the stress and the particle velocity relations which hold along the characteristics are given by

$$\sigma \pm (\rho c_1)u = \text{constant; along } \frac{\mathrm{d}x}{\mathrm{d}t} = \mp c_1 \tag{2}$$

and

$$\tau \pm (\rho c_2)v = \text{constant; along } \frac{\mathrm{d}x}{\mathrm{d}t} = \mp c_2. \tag{3}$$

In Eqs. (2) and (3), σ and τ are the normal and shear stresses, u and v are the normal and transverse components of the particle velocity, ρ is the mass density, and (ρc_1) and (ρc_2) are the longitudinal and shear impedance, respectively.

Using the initial conditions, it can be shown that all states at the impact face of an elastic flyer plate must satisfy the following characteristic relations:

$$\sigma + (\rho c_1)_{\mathrm{f}} u = (\rho c_1)_{\mathrm{f}} u_0 \tag{4}$$

and

$$-\tau + (\rho c_2)_{\mathrm{f}} v = (\rho c_2)_{\mathrm{f}} v_0. \tag{5}$$

Moreover, all states on the impact face of an elastic target plate must satisfy the following characteristic equations:

$$-\sigma + (\rho c_1)_{\mathrm{t}} u = 0 \tag{6}$$

and

$$\tau + (\rho c_2)_{\mathrm{t}} v = 0. \tag{7}$$

In Eqs. (4)–(7), the subscripts 'f' and 't' refer to the flyer and the target, respectively.

Using Eqs. (1)–(7), the components of traction at the interface between the flyer and the target can be expressed as:

$$\tau(t) = -\frac{(\rho c_2)_{\mathrm{t}}}{2} v_{\mathrm{fs}}(t) \tag{8}$$

and

$$\sigma(t) = \frac{(\rho c_1)_t}{2} u_{fs}(t), \tag{9}$$

where $v_{fs}(t)$ and $u_{fs}(t)$ are the transverse and the normal particle velocities at the rear surface of the target plate.

Based on the elementary definition of friction between two dry contact surfaces under no slip condition, the coefficient of static friction, μ_s, satisfies the inequality

$$\mu_s \geq \left| \frac{\tau}{\sigma} \right|. \tag{10}$$

For a fully elastic impact with no-slip at the interface, Eq. (10) provides a lower bound for the static coefficient of friction, μ_s. When slipping occurs at the flyer–target interface, the measured free surface velocity of the target plate can be used along with Eqs. (8) and (9) to obtain the coefficient of kinetic friction

$$\mu_k(t) = \left| \frac{\tau}{\sigma} \right|. \tag{11}$$

To calculate the interfacial slip velocity, the transverse particle velocity versus shear-stress diagram is utilized. The loci of all possible shear-stress and transverse particle velocity states, for a given flyer–target plate combination, are shown in Fig. 3. For a no-slip condition, the state of the interface is represented by the letter A. If the interface slip velocity is V_{slip}, the transmitted shear stress at the flyer–target interface is reduced from τ_A to $\tau*$. Consequently, the particle velocities on the flyer and the target sides of the interface are represented by V_B and V_C, respectively. Then, from the knowledge of the impact velocity V, the skew angle θ, the shear impedances of the flyer and the target plates, and the measured free-surface transverse velocity $v_{fs}(t)$, the slip velocity can be expressed as

$$V_{slip} = V_B - V_C = V \sin\theta - \left[\frac{(\rho c_2)_t + (\rho c_2)_f}{2(\rho c_2)_f} \right] v_{fs}(t). \tag{12}$$

The accumulated slip distance can be obtained from Eq. (12) by integrating the slip velocity in time

$$\delta_{slip} = \int_0^t V_{slip}(t) \mathrm{d}t. \tag{13}$$

Moreover, under conditions of no slip between the flyer and the target plates, the free surface particle velocities of the rear surface of the target plate are related to the flyer velocity by

$$u_{fs} = \frac{2(\rho c_1)_f}{[(\rho c_1)_t + (\rho c_1)_f]} V \cos\theta \tag{14}$$

and

$$v_{fs} = \frac{2(\rho c_2)_f}{[(\rho c_2)_t + (\rho c_2)_f]} V \sin\theta. \tag{15}$$

4.2. State 2

When the compressive longitudinal wave reflects from the free surface of the target plate, it reduces the compressive normal stress at the interface from σ_1 to σ_2

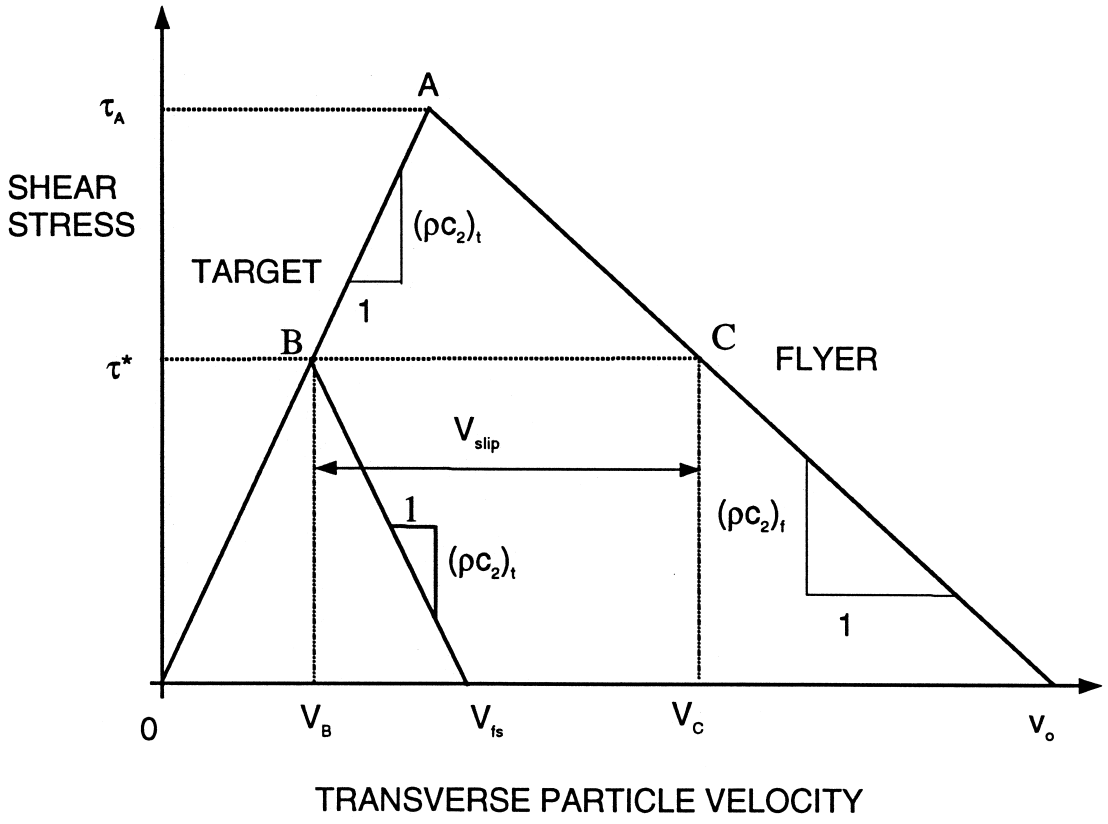

Fig. 3. Loci of all shear stress and transverse particle velocity states at the tribo–pair interface. Note that $V_{slip} = V_B - V_C$.

$$\sigma_2 = \frac{[(\rho c_L)_f - (\rho c_L)_t]}{[(\rho c_L)_f + (\rho c_L)_t]}\sigma_1. \tag{16}$$

For the Ti–6Al–4V/CH tool-steel tribo-pair employed in the present study, the ratio $\sigma_2/\sigma_1 \sim 0.33$.

The corresponding expressions for the friction stress and slip velocity can be obtained by solving the characteristic relations for State 2, and can be expressed as

$$\tau_2(t) = -\frac{(\rho c_2)_t}{2} v_B(t) \tag{17}$$

and

$$V_2^{slip} = V \sin\theta - \left[\frac{(\rho c_2)_t + (\rho c_2)_f}{(\rho c_2)_f}\right] v_B(t). \tag{18}$$

4.3. State 3

When the shear wave, reflected from the free surface of the target plate, arrives at the tribo-pair interface, it produces a change in friction state by altering the applied shear stress at the tribo-pair

interface while maintaining the same normal stress. Thus, the measurements made during State 3 are a direct probe of the relationship between the friction stress and slip velocity at constant normal pressure. The corresponding relations for interfacial tractions and slip velocity can be obtained by solving the characteristic relations for State 3, and can be expressed as

$$\tau_3(t) = -\frac{(\rho c_2)_t}{2}(v_C(t) - v_A(t)), \tag{19}$$

$$\sigma_3 = \sigma_2 \tag{20}$$

and

$$V_3^{slip} = V \sin\theta + \left[\frac{(\rho c_2)_t - (\rho c_2)_f}{(\rho c_2)_f}\right] v_A(t) - \left[\frac{(\rho c_2)_t + (\rho c_2)_f}{(\rho c_2)_f}\right] v_C(t). \tag{21}$$

5. Experimental results and discussion

Using the plate–impact pressure shear friction configuration, a series of experiments was conducted to study the interfacial friction behavior of a Ti–6Al–4V and Carpenter Hampden tool steel tribo-pair. Table 2 summarizes the five experiments conducted in the present study. In all these experiments, Ti–6Al–4V was used as the flyer plate and Carpenter Hampden tool-steel plate was used as the target. Additionally, the skew angle θ was kept constant at 35°. The frictional state at the tribo-pair interface was varied by varying the normal pressure and/or the surface roughness of the impacting surfaces. Moreover, by appropriate selection of the flyer and target plate thickness, the tribo-pair interface was subjected to step changes in normal pressure and step changes in applied shear stress.

Experiments SHOT 9701 and SHOT 9702 were designed to study the effect of normal pressure on interfacial frictional resistance of sliding interfaces. In view of this, the tribo-pair surfaces were kept relatively smooth and the impact velocity was varied to subject the tribo-pair interface to different levels of normal pressure. For SHOT 9701 and SHOT 9702, the surface roughness of Ti–6Al–4V plate was 0.07 and 0.09, respectively, whereas the surface roughness of the Carpenter Hampden tool-steel plate was maintained at 0.02 for both experiments. In order to vary the applied normal pressure, the impact velocity for SHOT 9701 was kept at 76 m/s ($\sigma_1 = 1.017$ GPa) whereas the impact velocity for SHOT 9702 was 95 m/s ($\sigma_1 = 1.292$ GPa). Experiments SHOT 9703 and SHOT 9704 were designed to study the effect of normal pressure on interfacial frictional behavior when the surface roughness of CH tool-steel plate (the harder plate in the tribo-pair) was increased substantially. In view of this, experiments SHOT 9703 and SHOT 9704 were conducted with surface roughness of 0.12 and 0.11, respectively, while the surface

Table 2
Summary of plate impact pressure shear friction experiments conducted in the present study

SHOT #	Skew angle θ	Impact velocity (m/s)	Normal stress (GPa)	Ti–6Al–4V roughness, Rq (μm)	C.H. steel roughness, Rq (μm)
9701	35°	76	1.017	0.1	0.02
9702	35°	95	1.292	0.07	0.02
9703	35°	102.7	1.374	0.09	0.12
9704	35°	80.5	1.078	0.09	0.11
9801	35°	79.2	1.059	0.18	0.10

roughness of the Ti–6Al–4V flyer plate was kept constant at 0.09 for both experiments. SHOT 9703 was conducted at 102.7 m/s whereas the impact velocity for SHOT 9704 was 80.5 m/s. Finally SHOT 9801 was conducted to study the effect of the increase in surface roughness of Ti–6Al–4V plate on the sliding resistance of the tribo-pair. For SHOT 9801 the surface roughness of Ti–6Al–4V was increased to 0.18 from 0.09, while the surface roughness of the Carpenter Hampden tool-steel plate was kept similar to the surface roughness of the Carpenter Hampden tool-steel plate employed in SHOT 9704. Moreover, the impact velocity for SHOT 9801 (79.2 m/s) was kept sufficiently close to the impact velocity employed in SHOT 9704 so as to keep the normal pressure the same in the two experiments.

In the following, experimental results obtained from pressure–shear experiments corresponding to SHOT 9702, SHOT 9703, SHOT 9704 and SHOT 9801 are described. Fig. 4 shows the free surface normal and transverse velocity history for SHOT 9702. The abscissa represents the time after impact. The compressive longitudinal wave arrives at the rear surface of the target at approximately 1100 ns. Upon arrival of the longitudinal wave, the normal particle velocity jumps to 55.8 m/s. This level correlates well with the elastic prediction given by Eq. (14). The rise time associated with this jump is approximately 5–10 ns. The second step rise in normal particle velocity occurs at approximately 2900 ns and is due to the arrival of the reflected longitudinal wave from the tribo-pair interface. This level of the normal particle velocity is consistent with the normal pressure drop at the frictional interface during the transition from State 1 to State 2. Thereafter, the normal particle velocity remains constant since the transition from State 2 to State 3 involves a change in the applied shear stress at the frictional interface while maintaining the same normal pressure.

The first arrival of shear wave at the free surface of the target plate occurs at approximately 1900 ns. The latter arrival of the shear wave relative to the longitudinal wave is consistent with a lower wave speed of the shear wave as compared to the longitudinal wave. The drop in free surface transverse particle velocity at approximately 3600 ns is due to the step drop in normal pressure and indicates the beginning of State 2. With the drop in normal pressure, a smaller level of transverse particle velocity is transmitted across the friction interface. The following rise in the free surface transverse particle velocity at approximately 5250 ns indicates the beginning of State 3. The dashed horizontal line represents the elastic prediction for the transverse particle velocity at the free surface of the target plate, had there been no slipping at the tribo-pair interface. Since the levels of the transmitted particle velocity in the

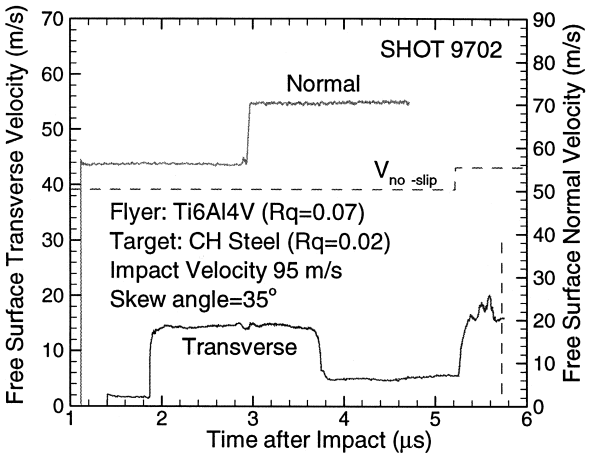

Fig. 4. Normal and transverse free surface particle velocity history at the rear surface of the target plate — Shot 9702.

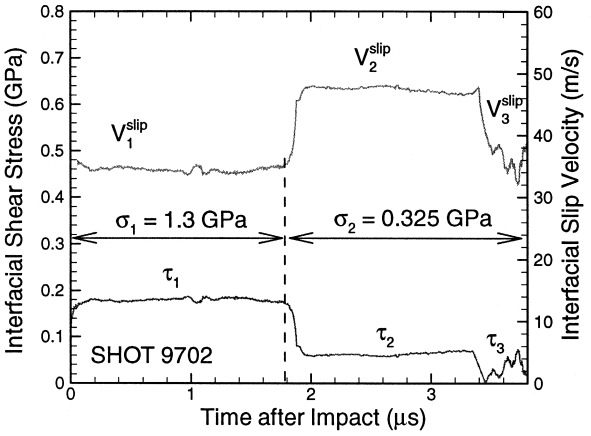

Fig. 5. Interfacial normal pressure, friction stress and slip velocity history — Shot 9702.

three states are much lower than their corresponding no-slip predictions, the frictional interface is understood to be in a state of dynamic slip.

Fig. 5 shows the history of the interfacial normal pressure, friction stress and interfacial slip velocity as a function of time for SHOT 9702. These quantities are obtained from the measured normal and transverse free surface particle velocity profiles depicted in Fig. 5 in conjunction with Eqs. (8)–(21). During State 1, the normal pressure σ_1 at the frictional interface is 1.3 GPa. Immediately after the application of pressure–shear loading, the frictional interface jumps to a state of steady state sliding characteristic of the surface roughness and the applied normal pressure. In this steady state, the transmitted shear stress τ_1 is approximately 0.18 GPa and the slip velocity V_1^{slip} is 34 m/s. The attainment of the steady frictional state is consistent with the results of the molecular dynamics simulations of Rigney and Hammerberg (1998) which clearly show that, for atomically smooth surfaces and relatively rough surfaces, a steady friction state is achieved very early in the loading process. The molecular dynamic simulations also show that, for atomically smooth surfaces, the evolution of the friction state to a steady state is preceded by a series of stick–slip events, which result in a wave structure in the transverse velocity field. However, the early time details of how a friction state evolves to a steady state have not been resolved experimentally, at present. For Shot 9702, the steady state continues up to 1800 ns, when the arrival of the unloading normal wave from the free surface of the target plate results in a step drop of normal pressure. During the transition form State 1 to State 2, the unloading longitudinal wave reduces the normal pressure from $\sigma_1 = 1.3$ GPa to $\sigma_2 = 0.325$ GPa in approximately 5–10 ns. It is interesting to note that the corresponding friction stress τ_2 does not follow this step drop in normal stress. Instead, the friction stress gradually approaches a new steady state level characteristic of the current state of the frictional interface. At the reduced normal pressure, the steady state friction stress is reduced to 0.06 GPa and the slip velocity V_2^{slip} increases to approximately 48 m/s. State 2 continues up to approximately 3300 ns, at which time the reflected shear wave from the free surface of the target plate arrives at the tribo-pair interface (State 3). The arrival of the unloading shear wave results in a change in the applied shear stress at the frictional interface while maintaining the same normal pressure. Thus, State 3 is an exclusive measure of the shear stress versus slip velocity relationship of the frictional interface at constant normal pressure. It is interesting to observe that a change in the applied shear stress at the interface results in a sharp drop in slip velocity, V_3^{slip}. Corresponding to this drop in slip velocity is an initial rapid decrease in the friction stress followed by a

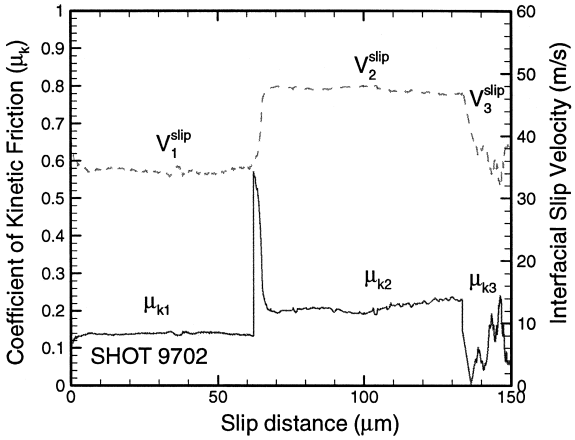

Fig. 6. Coefficient of kinetic friction and slip velocity as a function of interfacial slip distance — Shot 9702.

slow rise in friction stress to a new steady state level of τ_3. The evolution of frictional stress immediately following the arrival of the shear wave (transition form State 2 to State 3) is represented by a straight line since it is difficult to accurately resolve this regime from the present experimental measurements of the free surface transverse particle velocity histories. Also, the steady state level for State 3 is difficult to interpret in the present experiments because of the relatively short time window available for State 3 (only 0.3 μs).

Fig. 6 shows the coefficient of kinetic friction μ_k and the slip velocity for SHOT 9702 as a function of the accumulated slip distance. For SHOT 9702, the total accumulated slip is of the order of 150 μm. This small level of accumulated slip is due to the short time duration of the present experiments (approximately 3.74 μs) even though the slipping speeds are high (25 to 50 m/s). The coefficient of kinetic friction in State 1 is approximately 0.14. This value of μ_k is relatively low as compared to the reported value of 0.36 for the coefficient of friction between ground steel and Ti–6Al–4V specimens under 200 g of load (Bhushan and Gupta, 1991). A plausible reason for these low values of μ_k can be attributed to the high normal pressure combined with high slip speeds in the present experiments. In view of these interfacial conditions, the asperity–asperity contact regions are sheared so rapidly that the rate of heat generation is much faster than it can be conducted away. This heat produces thermal softening at the asperity–asperity junctions, thus reducing their shearing strength and leading to lower values of frictional stress (Bowden and Persson, 1960; Kragelsky, 1991; Irfan and Prakash, 1994). Another reason for the lower values of μ_k may be due to the fact that the sliding resistance of a frictional interface comprises of combined effects of adhesion between the flat surfaces and plowing by wear particles and surface asperities of the harder material in the softer material (Suh, 1986). For a particular interface, it is the relative contribution of these components which is responsible for the effective magnitude of μ_k. In the present plate impact experiments, the slipping speeds are high but the slip distances are small. This relative small slip rules out any significant contribution from wear at the interface. Since it has been postulated by many researchers that almost half the contribution to the sliding resistance evolves from debris formation and plowing during the slip process, it may not be surprising that the values of μ_k obtained in the experiments are much lower.

Furthermore, from Fig. 6 it can be inferred that during the transition from State 1 to State 2 there is an instantaneous jump in the value of coefficient of friction. This jump in μ_k is followed by a new steady state level. The jump in μ_k is understood to be due to the fact that the friction stress does not follow the

change in the applied normal pressure but instead evolves with slip (decays approximately exponentially) immediately after the step pressure change. The evolution of friction stress in response to a step change in normal pressure provides insight into the evolution of the effective area of contact and introduces a critical relaxation time to the dynamic friction process. Additionally, it is observed that the steady state level of the coefficient of kinetic friction in State 2 ($\mu_k \sim 0.22$) is much higher than the steady state level of μ_k in State 1 ($\mu_k \sim 0.14$). This is an important result and provides direct evidence in support of the fact that during high speed sliding, the steady-state friction stress may not decrease in proportion to the drop in normal pressure (Prakash, 1998a). Again, this result can be interpreted in terms of an effective area of contact and suggests that for the CH steel/Ti–6Al–4V tribo-pair, under the interfacial conditions prevailing in the present experiments, during the transition from one steady state to another the true area of frictional contact may not decrease in proportion to the change in the applied normal pressure.

However, it must be mentioned that the aforementioned experimental observation, i.e. the steady state coefficient of kinetic friction is higher in the frictional state after the step change in normal pressure as compared with the steady state coefficient of kinetic friction prior to the step pressure drop, was not observed in similar plate impact pressure–shear friction experiments conducted on WC/Ti–6Al–4V tribo-pair (Prakash, 1998a). In the experiments on the WC/Ti–6Al–4V tribo-pair, the level of the steady state coefficient of kinetic friction before and after the step pressure change were approximately the same, implying that, for the WC/Ti–6Al–4V tribo-pair, the *steady-state* friction stress changes approximately linearly with the applied normal pressure. It must be noted that the steady state conditions at the frictional interface were very different in the two experiments. The slip speeds for the experiments involving WC/Ti–6Al–4V tribo-pair were much smaller (approximately 10 m/s before the step pressure change and 30 m/s after the step pressure change) as compared to those obtained in SHOT 9702. Also, the normal pressure drop for the WC/Ti–6Al–4V tribo-pair was $\sigma_2/\sigma_1 \approx 0.5$ (from 2.0 GPa to 1 GPa) as compared to $\sigma_2/\sigma_1 \approx 0.33$ for the CH steel/Ti–6Al–4V tribo-pair in SHOT 9702. However, these differences in interfacial conditions are not expected to have a major influence on the observed response under discussion. These results are important, especially in view of the considerable efforts being devoted to understand the mechanics of high speed machining of Ti–6Al–4V alloys, and may provide an explanation for the much higher tool temperatures and tool wear observed while machining Ti–6Al–4V alloys with D3 tool steels as compared to machining Ti–6Al–4V with WC tools.

During State 3, the value of the coefficient of kinetic friction depicts the behavior discussed earlier for the evolution of friction stress in Fig. 6. The transition from State 2 to State 3 results in a sharp drop in slip velocity relative to the slip velocity in State 2. This sharp drop in slip velocity leads to an initial drop in friction stress, followed by an increase in the friction stress to a new steady state level. The level of friction stress in State 3 is only slightly different from the level in State 2. Similar frictional behavior was observed in dynamic friction tests by Dieterich (1978, 1979), Ruina (1983), Rice and Ruina (1983) and Dupont and Dunlap (1995). In their experiments, they observed that immediately after a fast upward (downward) jump of slip velocity, the tangential force increases (decreases) rapidly then decreases (increases) slowly to the new steady state value. This results in a force spike followed by relaxation over time which scales with the new slip speed, thus revealing a characteristic length lying in the micrometer range. Dieterich (1978, 1979) interpreted the transients in the experiments in terms of a memory length and argued that during non-steady slip of a frictional interface, the friction coefficient does not depend on the instantaneous slip velocity.

The bulk temperature rise at the tribo-pair interface is estimated by solving the following one dimensional transient heat conduction equation

$$\frac{\partial^2 T}{\partial x^2} = \frac{1}{\alpha}\frac{\partial T}{\partial t}, \tag{22}$$

with initial condition

$$T(x,0) = 0 \tag{23}$$

and boundary conditions

$$-k\frac{\partial T}{\partial x}(x = 0,\, t) = \dot{q}(t) \tag{24}$$

and

$$T(x = \infty,\, t) = 0. \tag{25}$$

In Eqs. (22)–(25), T is the temperature rise, k is the thermal conductivity, α is the thermal diffusivity and x represents the distance perpendicular to the interface. Using Eqs. (22)–(25), the temperature rise distribution as a function of time and position can be obtained as

$$T(x,\, t) = \frac{1}{k}\int_0^t \dot{q}(\xi)\frac{\sqrt{\alpha}}{\sqrt{\pi(t-\xi)}}\exp\left(\frac{-x^2}{4\alpha(t-\xi)}\right)\mathrm{d}\xi. \tag{26}$$

In order to calculate the temperature distribution in the tribo-pair, an estimate for the heat source $\dot{q}(t)$ is required. Using the experimentally measured frictional stress τ, and the slip velocity V_{slip}, the heat generated at the interface can be estimated to be

$$\dot{q}_{\text{Ti–6Al–4V}}(t) = \beta\tau(t)V_{\text{slip}}(t) \tag{27}$$

and

$$\dot{q}_{\text{CH steel}}(t) = (1-\beta)\tau(t)V_{\text{slip}}(t), \tag{28}$$

where β governs the partitioning of heat in the tribo-pair materials. The fraction β is estimated by equating the temperatures at the tribo-pair interface to yield

$$\beta = \frac{k_1\sqrt{\alpha_2}}{k_2\sqrt{\alpha_1} + k_1\sqrt{\alpha_2}}. \tag{29}$$

In Eq. (29), k_1, α_1, k_2 and α_2, are the thermal conductivity and thermal diffusivity of Ti–6Al–4V and CH Steel, respectively. Table 1 lists the thermal properties for the two materials. In view of Eq. (29), approximately 23% of the heat generated at the tribo-pair interface due to frictional sliding goes into Ti–6Al–4V and 77% of the heat goes into CH steel.

Bulk temperature estimates for Ti–6Al–4V and CH tool-steel (SHOT 9702) are illustrated in Fig. 7(a,b), respectively. The diffusive nature of the solution to Eq. (26) is clearly evident from the sharp decay in the bulk temperatures along with the loss in the high frequency information with increasing distance perpendicular to the frictional interface. The maximum temperature rise at the frictional interface during State 1 occurs at the transition from State 1 to State 2, and is approximately equal to 600°C. The interfacial temperatures during State 2 remain essentially constant at approximately 550°C during the entire duration of State 2. The lower interfacial temperatures in State 3 relative to State 2 is a consequence of the sharp decrease in the interfacial slip velocity in State 3 while the friction stress remains at essentially the same level as in State 2.

It must be mentioned that the aforementioned computed temperature rise distributions are an estimate of the actual global temperatures existing during the frictional sliding process. A number of assumptions have been made in arriving at these estimates:

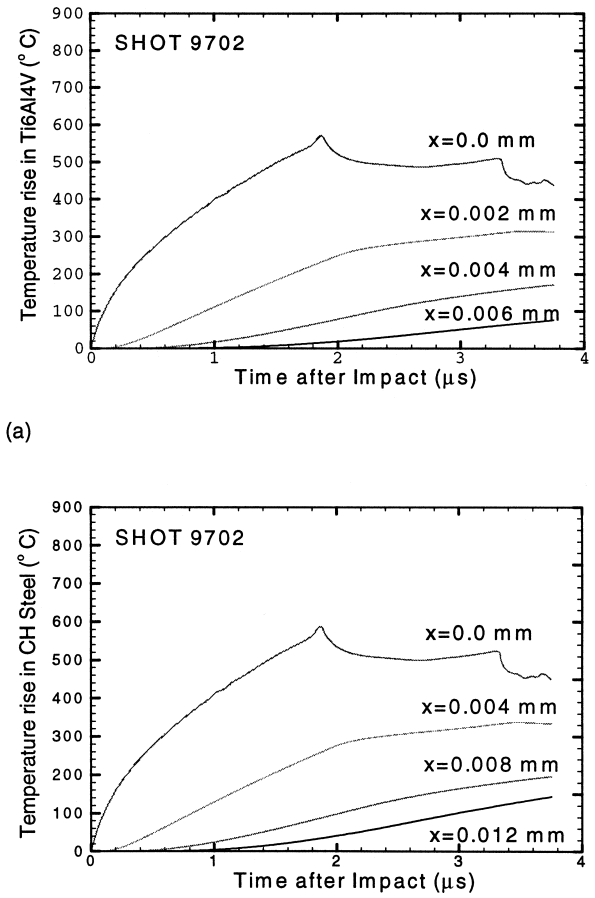

Fig. 7. Computed temperature rise for Shot 9702, (a) in Ti6Al4V, (b) in Carpentor Hampden tool steel.

(a) the thermal properties of the tribo-pair materials are assumed to be constant at their room temperature values at all temperatures, and
(b) all the interfacial frictional work is assumed to be converted to heat.

The assumption that all the frictional work is converted to heat is expected to lead to an overestimation of the actual tribo-pair temperature rise distribution. However, it must be recalled that in the present experiments, the impact velocity is controlled such that both the flyer and the target materials remain elastic during the entire duration of the experiment. Thus, all inelastic processes during the pressure shear loading are expected to occur within a thin layer at the frictional interface, the thickness of which is of the order of the surface roughness of the tribo-pair materials. In view of these arguments, the computed temperature profiles are expected to represent the actual temperature distributions with an acceptable level of accuracy.

The experimental results for SHOT 9703 are presented in Figs. 8–10. In this experiment, the surface roughness of the Carpenter Hampden steel plate was 0.12, which is approximately six times greater than the roughness of the target plate employed in SHOT 9702. The *Rq* value of the Ti–6Al–4V flyer was 0.09, which is approximately the same as the surface roughness of the Ti–6Al–4V plate employed in SHOT 9702. Fig. 8 shows the history of the friction stress and interfacial slip velocity as a function of

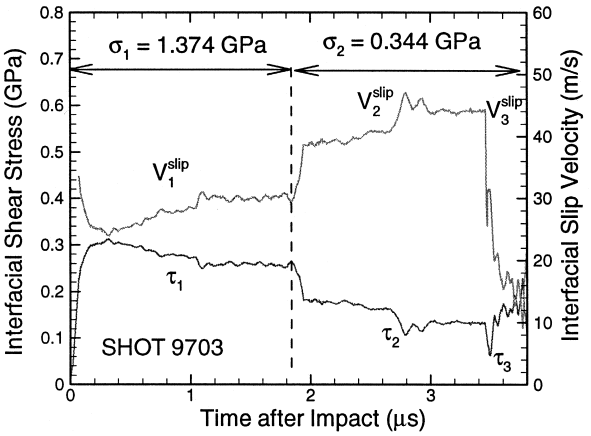

Fig. 8. Interfacial normal pressure, friction stress and slip velocity history — Shot 9703.

time after impact for SHOT 9703. During State 1, the normal pressure σ_1 at the interface was 1.374 GPa. It is interesting to note the absence of steady-state friction during State 1 and the friction stress is observed to decay steadily with slip. This non-steady friction state is understood to be a result of the higher surface roughness of the CH steel plate (0.12) combined with the higher impact velocity (102.7 m/s) employed in SHOT 9703. The presence of higher initial surface roughness and higher normal pressures leads to a decrease in friction resistance with slip due to smoothening of the interface with slip and hence to a state of dynamic slip instability at the interface. It must be reiterated that in experiments SHOT 9701 and SHOT 9702, for which the surface roughness of the tribo-pair materials was relatively smooth, steady state conditions were obtained at both high and low normal pressures. The average value of the frictional stress during State 1 for SHOT 9703 was approximately 0.3 GPa, which is relatively higher than the frictional stress transmitted in SHOT 9702. The higher level of friction stress is attributed to the higher surface roughness of the target plate and higher normal pressures employed in SHOT 9703. During the transition from State 1 to State 2, the unloading longitudinal wave reduces the normal pressure from 1.374 GPa to 0.344 GPa in approximately 5–10 ns. As also noted for SHOT 9702,

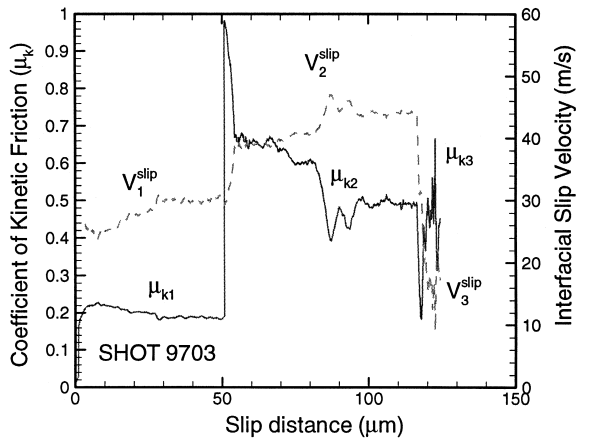

Fig. 9. Coefficient of kinetic friction and slip velocity as a function of interfacial slip distance — Shot 9703.

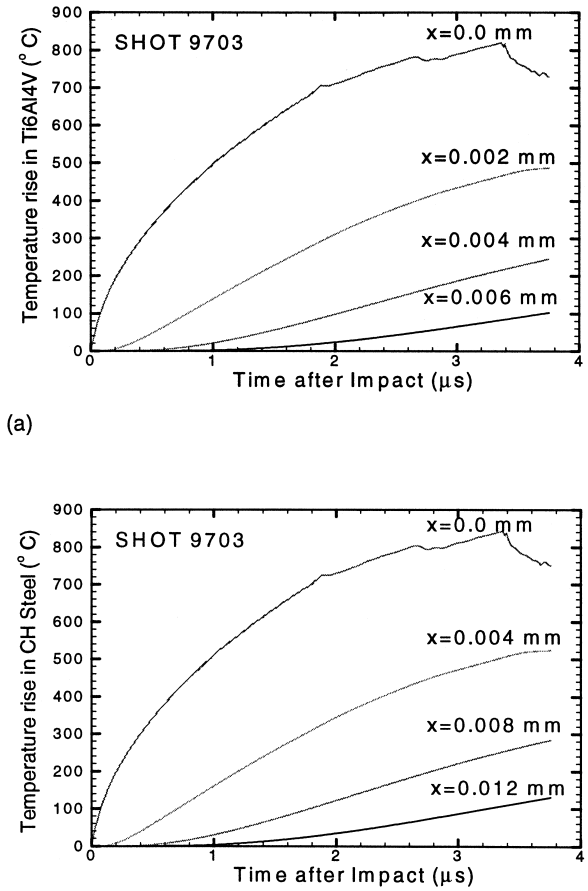

Fig. 10. Computed temperature rise for Shot 9703, (a) in Ti6Al4V, (b) in Carpentor Hampden tool steel.

the friction stress τ_2 does not follow this step drop in normal stress. In fact, the friction stress gradually evolves towards a new friction state characteristic of the current normal pressure and slip velocity. At the reduced normal pressure, the average friction stress is reduced to 0.16 GPa and the slip speed V_2^{slip} increases to approximately 45 m/s. In State 3, a drop in slip velocity (V_3^{slip}) at the interface leads to an initial rapid decrease in friction stress followed by a slow rise to a steady state level τ_3, as also observed in SHOT 9702.

Fig. 9 shows the evolution of coefficient of kinetic friction μ_k and slip velocity for SHOT 9703 as a function of accumulated slip distance. The average value for the coefficient of kinetic friction in State 1 is approximately 0.2. As discussed for SHOT 9702, during the transition from State 1 to State 2, there is an instantaneous jump in the value of the coefficient of kinetic friction, followed by an evolution towards a new level. The coefficient of kinetic friction in State 1 just prior to the step pressure change is 0.22, while the coefficient of kinetic friction in State 2 just after the pressure change is 0.55. The interfacial temperature for SHOT 9703 [Fig. 10(a,b)] are much higher (approximately 700°C) as compared to those obtained in SHOT 9701 (approximately 400°C) and SHOT 9702 (approximately 600°C). It is interesting to note that even though the normal pressure drop is the same in both experiments, the combination of higher normal pressure in State 2 and higher interfacial temperatures

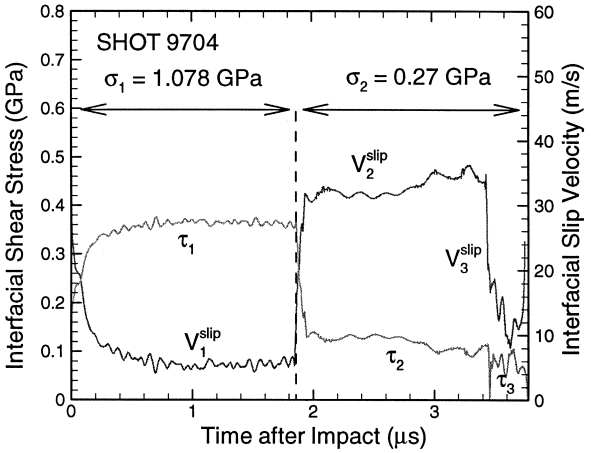

Fig. 11. Interfacial normal pressure, friction stress and slip velocity history — Shot 9704.

just prior to the step drop in normal pressure allow a much smaller decrease in the effective area of contact and hence to a higher coefficient of kinetic friction ratio for SHOT 9703 ($\mu_{k_2}/\mu_{k_1} \sim 3$) as compared to SHOT 9702 ($\mu_{k_2}/\mu_{k_1} \sim 1.8$). During State 3, the value of the coefficient of kinetic friction depicts the behavior discussed earlier for SHOT 9702.

The experimental results for SHOT 9704 are presented in Figs. 11–13. In this experiment, the surface roughness of the Carpenter Hampden steel and the Ti–6Al–4V plates were approximately similar to those employed in SHOT 9703. However, the impact velocity for Shot 9704 was reduced to 80.5 m/s, as compared to 102.7 m/s for SHOT 9703. Fig. 11 shows the history of friction stress and interfacial slip velocity as a function of time after impact for SHOT 9704. During State 1, the normal pressure σ_1 at the interface was 1.078 GPa. It is interesting to note that in SHOT 9704, by decreasing the applied normal pressure while maintaining the same surface roughness as the tribo-pair surfaces employed in Shot 9703, a steady-state interfacial slip condition is again obtained at the frictional interface. This observation reinforces the earlier claim that it is the combination of higher surface roughness and higher

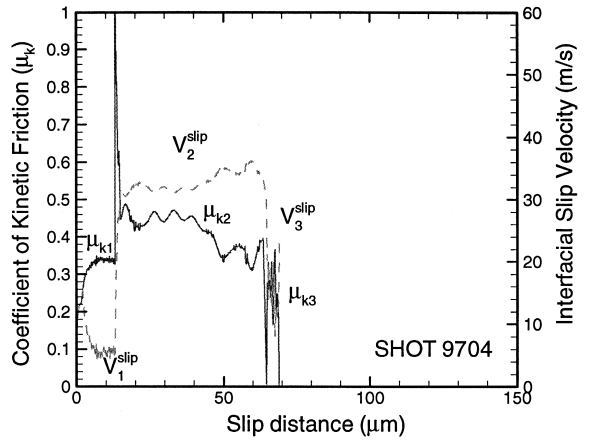

Fig. 12. Coefficient of kinetic friction and slip velocity as a function of interfacial slip distance — Shot 9704.

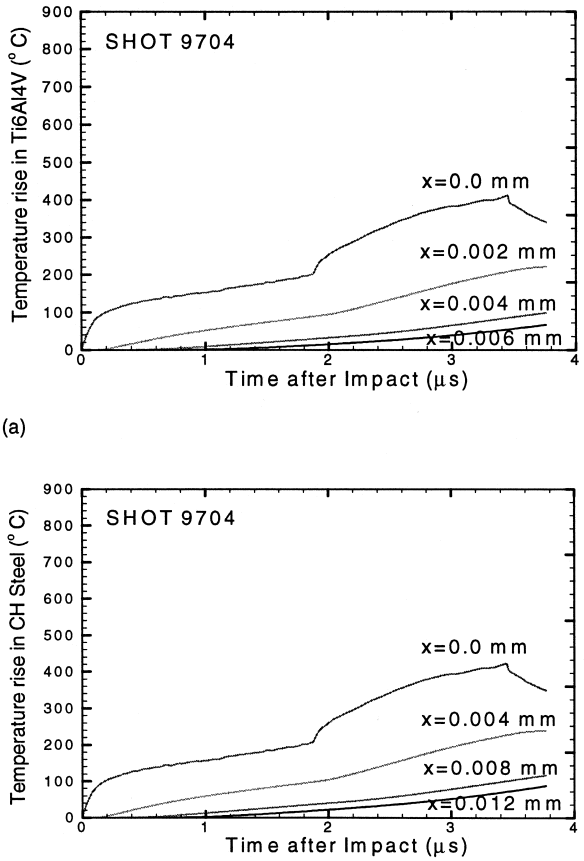

Fig. 13. Computed temperature rise for Shot 9704, (a) in Ti6Al4V, (b) in Carpentor Hampden tool steel.

normal pressures that leads to dynamic slip instability at the frictional interface. The average value of the friction stress during State 1 is approximately 0.37 GPa, which is relatively higher than the frictional stress transmitted in SHOT 9703. During transition from State 1 to State 2, the unloading longitudinal wave instantaneously reduces the normal pressure from 1.078 GPa to 0.27 GPa. As also noted for SHOT 9702 and SHOT 9703, the friction stress τ_2 does not follow the step drop in normal stress and gradually evolves towards a new frictional state characteristic of the current normal pressure and current slip velocity. After the normal pressure drop, the level of the steady-state friction stress is reduced to 0.14 GPa and the steady-state slip velocity increases to 34 m/s. In State 3, a drop in slip velocity (V_3^{slip}) at the interface leads to an initial rapid decrease in friction stress followed by a slow rise to a steady state level (τ_3), as also observed in SHOT 9702 and SHOT 9703.

Fig. 12 shows the evolution of the coefficient of kinetic friction μ_k and slip velocity for SHOT 9704 as a function of accumulated slip distance. The average value for the coefficient of kinetic friction in State 1 is approximately 0.35. As discussed for SHOT 9702 and SHOT 9703, during the transition from State 1 to State 2, there is an instantaneous jump in the value of coefficient of kinetic friction followed by an evolution towards a new steady state level. Also, for SHOT 9704, the coefficient of kinetic friction at the beginning of State 2 is higher than the level of μ_k prior to the step change in normal pressure

($\mu_{k_2}/\mu_{k_1} \sim 1.2$). Because of the relatively smaller slip speeds obtained during SHOT 9704, the interfacial temperatures for SHOT 9704 [Fig. 13(a,b)] are much smaller (approximately 230°C) as compared to those obtained in SHOT 9701 (approximately 400°C), SHOT 9702 (approximately 600°C) and SHOT 9703 (approximately 700°C). It is interesting to note that even though the normal pressure drop remains the same for the three experiments, the combination of lower interfacial temperatures (just prior to the normal pressure drop) and lower applied normal pressure in State 2 result in a lower coefficient of kinetic friction ratio for SHOT 9704 ($\mu_{k_2}/\mu_{k_1} \sim 1.2$) as compared to SHOT 9702 ($\mu_{k_2}/\mu_{k_1} \sim 1.8$) and SHOT 9703 ($\mu_{k2}/\mu_{k1} \sim 3$). During State 3, the value of the coefficient of kinetic friction depicts the behavior discussed earlier for SHOT 9702.

The experimental results for SHOT 9801 are presented in Fig. 14. For SHOT 9801, the surface of the Ti–6Al–4V was increased to 0.18, whereas the surface roughness of the Carpenter Hampden tool-steel plate was kept similar to the roughness of the Carpenter Hampden tool-steel plate employed in SHOT 9704. Moreover, the impact velocity for SHOT 9801 (79.2 m/s) was kept sufficiently close to the impact velocity employed in SHOT 9704 so as to keep the applied normal pressure the same in the two experiments. Fig. 14 shows the free surface normal and transverse velocity history for SHOT 9801. The abscissa represents the time after impact. During State 1, the normal pressure σ_1 at the interface was 1.059 GPa. It should be noted that by increasing the surface roughness of the Ti–6Al–4V plate while maintaining the same normal pressure as in Shot 9704, the non-steady friction state observed in SHOT 9703 is again obtained. This result reinforces the earlier observation that the presence of higher surface roughness can generate conditions conducive to dynamic slip instability at the frictional interface. It is also interesting to note that smoothening of the Ti–6Al–4V plate (softer of the two materials in the tribo-pair) can occur at a much lower normal pressures as compared to the CH tool steel plate in SHOT 9703, and thus the initially large surface roughness of Ti–6Al–4V plate leads to a non-steady slip state in SHOT 9801 at much lower pressures. The large step decrease in the magnitude of the free surface transverse particle velocity observed in State 2 is due to a small tilt during impact for this particular experiment. However, the measured free surface particle in State 1 is not affected by the presence of tilt

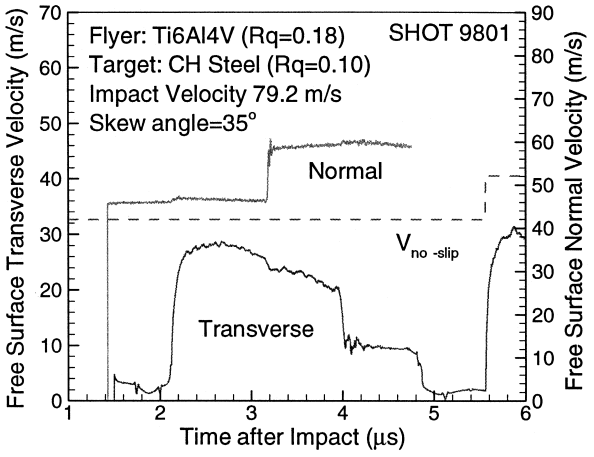

Fig. 14. Normal and transverse free surface particle velocity history at the rear surface of the target plate — Shot 9801.

(Prakash, 1998b) and the experimental results obtained in State 2 can be effectively used to infer the interfacial conditions.

6. Summary of the plate impact pressure–shear friction experiments

Pressure–shear plate impact friction experiments are conducted to study dynamic friction under interfacial normal pressures of 1–2 GPa, slip speeds of the order of 60 m/s, and interfacial temperatures of approximately 800°C at the frictional interface. By an appropriate design of flyer and target dimensions, the experiment has been effectively used to investigate the frictional resistance of sliding interfaces to step changes in normal pressure and step changes in applied shear stress.

The following conclusions can be deduced from the current experimental study.

1. The coefficient of kinetic friction μ_k is observed to decrease with an increase in normal pressure and interfacial slip speed when compared to that measured under quasi-static slip conditions.
2. For the Ti–6Al–4V/CH-steel tribo-pair, under the interfacial conditions existing in the present experiments, μ_k increases with the surface roughness of the impacting plates.
3. For relatively smooth tribo-pair surfaces, a state of steady frictional slip is achieved immediately after the pressure shear loading.
4. A combination of high surface roughness and high interfacial pressures is conducive to the development of slip instability at the frictional interface.
5. The measured interfacial shear stress shows frictional memory effects as a result of which μ_k jumps immediately following a step drop in normal pressure. This observation can also be interpreted in terms of a critical relaxation time involved with frictional slip.
6. During the transition from State 1 to State 2 (transition from high to low interfacial pressures), the level of coefficient of kinetic friction in State 2 (μ_{k_2}) is observed to be consistently greater than the steady-state level of coefficient of kinetic friction in State 1 (μ_{k_1}). Moreover, interfacial temperatures are observed to influence the μ_{k_2}/μ_{k_1} ratio.
7. A drop in interfacial slip velocity leads to an initial drop in transmitted shear stress followed by a gradual evolution towards a new steady state. Additionally, large changes in slip velocity are observed to lead to relatively small changes in the steady state friction stress.

Most conventional dynamic friction laws assume a linear dependence of the friction stress on the normal pressure. Also, friction memory effects are reflected in terms of static aging through the time of stationary contact, and dynamic aging which only includes the effects of changes in slip velocity. However, in view of the present experimental results, the functional dependence of the friction stress on the normal pressure needs to be included in the constitutive laws for dynamic friction. The constitutive laws should include the effects of the observed gradual evolution of the friction stress with changes in applied normal pressures and that steady state coefficients of kinetic friction can be pressure- and temperature-dependent. The nature of these transients separating the steady states are of great importance to geologists in the prediction of fault instabilities and to manufacturing engineers concerned with the stability of the tool/die workpiece interface during high speed manufacturing processes.

Acknowledgements

The authors would like to thank the Surface science and Tribology division of the National Science Foundation for support extended in carrying out this research.

References

Antoniou, S., Cameron, A., Gentle, C., 1976. The friction–speed relation from stick–slip data. Wear 36, 235–254.

Armstrong-Helouvry, B., Dupont, P., Canudas de Wit, C., 1994. A survey of models, analysis tools and compensation methods for the control of machines with friction. Automatica 30 (7), 1083–1153.

Bell, R., Burdekin, M., 1969. A study of stick–slip motion of machine tool feed drives. In: Proceedings Institute of Mechanical Engineers, vol. 184, pp. 543–560 Part I (30).

Bhushan, B., Gupta, B.K., 1991. Handbook of Tribology: Material Coatings and Surface Treatments. McGraw Hill Inc, NY.

Bowden, F.P., Freitag, E.H., 1958. The friction of solids at very high speeds, I. Metal on metal, II. Metal on diamond. Proceedings of the Royal Society of London A248, 350–367.

Bowden, F.P., Persson, P.A., 1960. Deformation heating and melting of solids in high speed friction. Proceedings of the Royal Society of London A260, 433–458.

Dieterich, J.H., 1978. Time dependent friction and mechanics of stick–slip. Pure and Applied Geophysics 116, 668–675.

Dieterich, J.H., 1979. Modeling of rock friction: I, experimental results and constitutive equations. Journal of Geophysical Research 84, 2161–2168.

Dupont, P., Dunlap, E., 1995. Friction modeling and PD compensation at very low velocities. ASME Journal of Dynamic Systems 117 (1), 8–14.

Irfan, M.A., Prakash, V, 1994. Contact temperatures during sliding in pressure shear impact. In: Proceedings, Society of Experimental Mechanics Conference. SEM, USA, pp. 173–182.

Kim, K.S., Clifton, R.J., Kumar, P., 1977. A combined normal and transverse displacement interferometer with an application to impact of Y-cut Quartz. Journal of Applied Physics 48, 4132–4139.

Kragelsky, V., 1991. Friction Wear and Lubrication, Tribology Handbook. Pergamon Press, Mir Publishers, Moscow.

Kumar, P., Clifton, R.J., 1977. Optical alignment of impact faces for plate impact experiments. Journal of Applied Physics 48, 1366–1367.

Martins, J.A.C., Oden, J.T., Simones, F.M.F., 1990. A study of static and kinetic friction. International Journal of Engineering Science 28, 29–92.

Ogawa, K., 1997. Impact friction test method by applying stress wave. Experimental Mechanics 37 (4), 398–402.

Prakash, V., 1995. A pressure–shear plate impact experiment for investigating transient friction. Experimental Mechanics 35 (4), 329–336.

Prakash, V., 1998a. Friction response of sliding interfaces subjected to time varying normal pressures. Journal of Tribology 120, 97–102.

Prakash, V., 1998b. Time-resolved friction with applications to high speed machining: experimental observations. Tribology Transactions 41 (2), 189–198.

Prakash, V., Clifton, R.J., 1993. Time resolved dynamic friction measurements in pressure shear. In: Ramesh, K.T. (Ed.), Experimental Techniques in the Dynamics of Deformable Bodies, AMD vol. 165. ASME, pp. 33–48.

Rajagopalan, S., 1999. Developement of a modified torsional Kolsky bar to study dynamic friction. MS Thesis, Case Western Reserve University, Cleveland, OH.

Rajagopalan, S., Irfan, M.A., Prakash, V., 1999. Novel experimental techniques for investigating time resolved high speed friction. Wear 225–229, 1222–1237.

Rice, J.R., Ruina, A., 1983. Stability of steady frictional sliding. Journal of Applied Mechanics 50, 343–349.

Rigney, D.A., Hammerberg, J.E., 1998. Unlubricated sliding behavior of metals. MRS Bulletin 23 (6), 32–36.

Roder, J., Hammerberg, J.E., Holian, B.L., Bishop, A.R., 1998. Multichain Frenkel–Kontorova model for interfacial slip. Physical Review B 57 (5), 2759–2766.

Ruina, A., 1983. Slip stability and state variable friction laws. Journal of Geophysical Research 88 (B12), 10359–10370.

Suh, N.P., 1986. Tribophysics. Prentice Hall, Englewood Cliffs, NJ.

Tanimura, S., Kaizu, K., Kawabata, H., 1989. Fundamental study of impact friction. Japanese Society of Mechanical Engineers 849 (1), 79–80.